Estimation of Acoustic Impedance from Multiple Ultrasound Images with Application to Spatial Compounding

Christian Wachinger[1], Ramtin Shams[2], Nassir Navab[1]

[1]Computer Aided Medical Procedures (CAMP), Technische Universität München, Germany
[2]Research School of Information Sciences and Engineering (RSISE), The Australian National University
wachinge@in.tum.de, ramtin.shams@anu.edu.au, navab@in.tum.de

Abstract

Reflection of sound waves, due to acoustic impedance mismatch at the interface of two media, is the principal physical property which allows visualization with ultrasound. In this paper, we investigate reconstruction of the acoustic impedance from ultrasound images for the first time. Similar to spatial compounding, we combine multiple images to improve the estimation. We use phase information to determine regions of high reflection from an ultrasound image. We model the physical imaging process with an emphasis on the reflection of sound waves. The model is used in computing the acoustic impedance (up to a scale) from areas of high reflectivity. The acoustic impedance image can either be directly visualized or be used in simulation of ultrasound images from an arbitrary point of view. The experiments performed on in-vitro and in-vivo data show promising results.

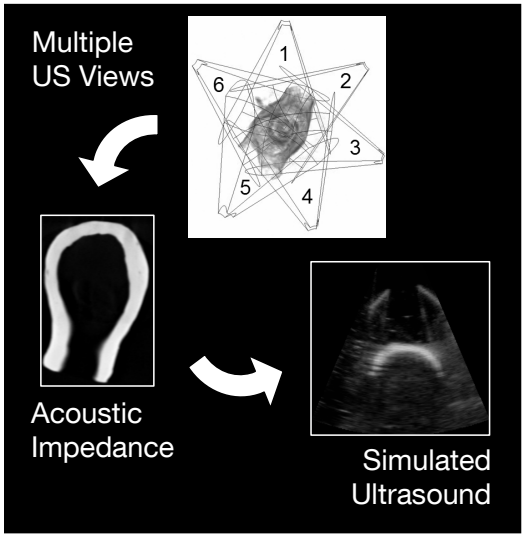

Figure 1. Schematic illustration of spatial compounding with acoustic impedance estimation. First, the impedance is estimated from multiple ultrasound images. Second, an ultrasound image is simulated from an arbitrary point of view.

1. Introduction

Ultrasound (US) has many advantages in comparison to other imaging modalities which has lead to its widespread use in clinical practice; it is (i) harmless at low power, (ii) portable, (iii) a real-time modality, and (iv) most importantly, cost effective. The recent introduction of 2D array US transducers in the market makes further applications possible, due to the instantaneous acquisition of ultrasound volumes. Furthermore, the next generation of transducers with CMUT[1] technology offers superior and efficient volumetric imaging at a lower cost. However, ultrasound has a number of disadvantages including: (i) a limited field-of-view (FOV), (ii) occlusions behind structures with high acoustic impedance, and (iii) a low singal-to-noise ratio (SNR). Spatial compounding of several views, acquired from different positions, helps to reduce these shortcomings.

The prerequisite for spatial compounding is to know the relative positions of the acquired images. This can either be obtained by tracking the ultrasound transducer or by image registration. When working with 2D US images compounding from different positions poses a problem, because all the scans have to be in one plane. Therefore, multi-angle compounding with beam steering is typically performed, where the probe remains fixed [22]. Moving to 3D imaging, compounding from different positions offers much more flexibility, inspiring several groups to work on this subject *e.g.* [6, 20]. In the following, we assume that we know the alignment of the images, and focus on how to combine their intensity information. As we will discuss later in this re-

[1]Capacitive Micromachined Ultrasound Transducer

978-1-4244-2340-8/08/$25.00 ©2008 IEEE

port, combining ultrasound images is non-trivial due to the highly view-dependent nature of the ultrasound. We will introduce a novel approach, which is based on the estimation of the acoustic impedance of the imaged scene. From each image, we will reconstruct an acoustic impedance image, which we subsequently average to get an estimation for the whole imaged area, see Figure 1. These images can either be directly presented to the physician or can be used in simulation of ultrasound images from an arbitrary point of view. To the best of our knowledge, this is the first time that acoustic impedance is reconstructed from multiple ultrasound images.

1.1. Clinical Value of Compounding

The clinical value of US compounding is mainly a result of increased quality and extended FOV of the images presented to the physician. When scanning the same region from different positions, speckle noise, which is direction dependent, can be reduced and therefore the SNR is improved [22]. Moreover, occlusion artifacts below structures with high acoustic impedance can be removed and the boundary continuity is enhanced. The positive effects of spatial compounding for diagnosis of atherosclerotic plaques [12, 13] and breast cancer [2] have already been reported. It also helps for administering epidural anesthesia by especially improving the depiction of key structures such as ligamentum flavum and epidural space [19]. Grau *et al*. [8] work on the combination of several acquisitions from different positions of the heart. It is not possible to depict the whole heart in a single acquisition, however, scans from particular acoustic windows can be acquired to show specific cardiac structures. The combination of these acquisitions into a single volume can be of great benefit in clinical practice.

The extended FOV is also of clinical value. First, sonographers have the flexibility to visualize anatomical structures from a variety of different angles [17]. Second, the spatial relationship among structures that are too large for a single volume is easier to understand [14]. Third, size and distance measurements of large organs are possible [14]. Fourth, individual structures within a broader context can be identified by having an image of the whole examination area [4]. And last, due to the increased features in the compounded view, specialists that are used to other modalities can better understand the spatial relationship of anatomical structures [10]; helping to bridge the gap between the modalities and making it easier to convey sonographic findings to other experts.

1.2. Related Work

The major problem in compounding ultrasound images, is the combination of US intensity values from different scans. If we were dealing with several computed tomography (CT) images of the same object, the compounding could be done by calculating the mean value. The dominant features of ultrasound due to reflection and attenuation are, however, view-dependent. Averaging intensity values is not optimal because strong echoes from small incident angles (transducer perpendicular to the surface) would be degraded by weak echoes from large incidence angles. Therefore, in the literature, several methods for spatial compounding have been proposed, which we are going to discuss shortly.

Wilhjelm *et al*. [22] use multi-angle spatial compounding with beam steering, for which the transducer stays at the same spatial location. They were able to reduce the angle dependency and speckle noise by combining multiple images. They compared a number of methods for compounding including mean, median, root-mean-squared value, and geometric mean. The highest SNR was achieved when using the mean method. In a recent work also based on beam steering, Tran *et al*. [19] improved the spatial compounding by using a combination of median- and gradient-based approaches. The median is used if at a certain location more than half of the images have a high feature-content, otherwise the gradient-weighted average is calculated. The problem we see with this approach is the use of thresholding to decide whether a pixel has a high feature-content or not. Behar *et al*. [3] propose a new method for spatial compounding by using three ultrasound transducers simultaneously. The transducer in the middle acts as sender and receiver, the remaining two only act as receiver. With their method they were able to improve visibility, detectability, and lateral resolution. During their experiments, various averaging methods were investigated, with the best results for the averaging of intensities.

Leotta and Martin [15] propose a weighting scheme based on the incidence angle of the ultrasound beam on a reflecting surface. This technique leads to significantly improved results in comparison to using the mean value, but is based on an initial fitting of a surface to the data, which is a challenge for complex images. Grau *et al*. [8] use multiscale information about local structure definition and orientation to weight the contributions of different images. The way they obtain these image characteristics is by calculating the image phase, which is invariant to image contrast being particularly interesting for US images. While this approach is very interesting for image registration [7], the compounding is rather cumbersome [8]. As can be seen, ultrasound compounding is a non-trivial exercise and still an active field of research.

1.3. Outline

In this article, we will present a new approach for compounding, based on the estimation of acoustic impedance of the depicted region. This has the advantage that the av-

eraging becomes a less complex task, because the acoustic impedance images are less view-dependent than the original US images. Once the acoustic impedance image is estimated, we can either present it directly or simulate ultrasound images from an arbitrary position. We describe the physical process of ultrasound imaging, our ultrasound model, and the actual estimation in Section 2. Our experiments together with the results are shown in Section 3.

2. Method

Core to our method is the estimation of the acoustic impedance of the region depicted in the ultrasound image. As we will see, acoustic impedance images are related to CT attenuation values expressed in Hounsfield units and no longer exhibit view-dependent artifacts and emphasized interface boundaries as in ultrasound images. Having the acoustic impedance images z_i from all views, the creation of a global acoustic impedance image z for the whole imaging scenario is possible.

2.1. Maximum Likelihood Estimation

The acoustic impedance estimation can be formulated as a maximum likelihood (ML) estimation. Therefore, we have to define an US simulation function s, producing one of the n simulated US images $\hat{\mathcal{U}} = \{\hat{u}_1, \ldots, \hat{u}_n\}$, by taking the corresponding transformation in $\mathcal{T} = \{T_1, \ldots, T_n\}$ and the acoustic impedance image z:

$$s : (z, T_i) \longmapsto \hat{u}_i. \tag{1}$$

The likelihood function, which indicates how well the simulated US images $\hat{\mathcal{U}}$ match the real ones $\mathcal{U} = \{u_1, \ldots, u_n\}$, is

$$\begin{aligned} \mathcal{L}(z) &= P(\mathcal{U}|z, \mathcal{T}, \varepsilon) && (2)\\ &= \prod_i P(u_i|z, T_i, \varepsilon) && (3)\\ &= \prod_i P(u_i - s(z, T_i) = \varepsilon), && (4) \end{aligned}$$

with the random variable ε modeling the noise and the assumption of independent US images. In order to proceed with the ML estimation $\arg\max_z \mathcal{L}(z)$, we have to choose a distribution for the noise.

Ultrasound speckle, in general, has a Rayleight distribution, however since we remove speckle as a preprocessing step, a Gaussian distribution to model the noise in the images is more appropriate, which leads to the following least-squares formulation

$$\log \mathcal{L}(z) \propto -\frac{1}{n} \sum_{i=1}^{n} \left(u_i - s(z, T_i)\right)^2. \tag{5}$$

In the next section we will describe details of ultrasound imaging to derive s.

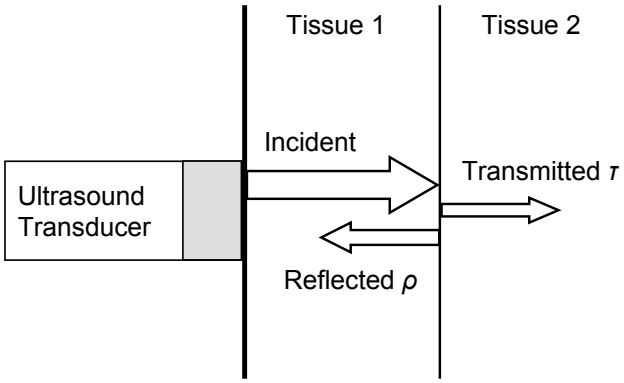

Figure 3. Reflection and transmission of sound wave after hitting an interface. The relative intensities are determined by the acoustic impedances of the tissues.

2.2. Physics of Ultrasound

In order to be able to estimate the acoustic impedance from an ultrasound image, we need a model of the physical imaging process. A detailed description of ultrasound physiscs can be found in [9]. Ultrasound waves are emitted into the body to interact with the tissue, and the results are presented for diagnosis in the form of reflected ultrasound waves. There are many types of interactions, but the most important ones, we are focusing on, are: reflection, scattering, and absorption. If the ultrasound beam hits an interface between two tissues with different acoustic impedances, Z_1 and Z_2, at normal incidence, part of the beam is reflected, expressed by the reflection coefficient ρ:

$$\rho = \left(\frac{Z_2 - Z_1}{Z_2 + Z_1}\right)^2. \tag{6}$$

The transmission coefficient τ is then given by:

$$\tau = 1 - \rho = \frac{4 \cdot Z_2 \cdot Z_1}{(Z_2 + Z_1)^2}. \tag{7}$$

This type of reflection is called specular reflection (see Fig. 3). One speaks of diffuse reflection if the beam is reflected in multiple directions, happening when a rough-surfaced interface is hit.

Scattering is responsible for providing the internal structure of the tissue and occurs when the beam hits interfaces smaller than the size of its wavelength. Each of these scatterers reflects sound in all directions, causing speckle. Absorption, as well as scattering, is frequency dependent and follows an exponential function

$$P(x) = P_{\text{max}} \cdot e^{-\alpha x} \tag{8}$$

with P_{max} the initial sound pressure, $P(x)$ the pressure after traversed distance x, and α the absorption coefficient. Scattering and absorption affect *attenuation*, which characterizes the amplitude reduction as the wave propagates

(a) Original US image (b) Phase image (c) Threshold of phase image (d) Impedance estimation (e) Smooth imp. estimation

Figure 2. Processing steps for acoustic impedance estimation of a clay model.

through a medium. Attenuation can also be described by an exponential function similar to Equation (8), only replacing the absorption coefficient α by an attenuation coefficient β, which is the sum of the scattering and absorption coefficients.

Ultrasound imaging can then be described by the reflection at tissue interfaces and the exponential loss of intensity within the tissue. Wein *et al*. [21], propose a model to simulate US from CT, by mapping CT Hounsfield units to acoustic impedance values. We can directly use this model without the need for a mapping. Following the model, a simulated ultrasound image $\hat{u}$ is made up from a reflection part r, an echogeneity part e, and a constant part, weighted with parameters ω_i

$$\hat{u}(\mathbf{x}) = \omega_1 \cdot r(\mathbf{x}) + \omega_2 \cdot e(\mathbf{x}) + \omega_3. \tag{9}$$

Like mentioned, we focus on the regions of high reflection, where the echogeneity can be ignored. The intensity of the sensed reflected signal R at a position $\mathbf{x}$ is calculated by running along the scan line with direction $\mathbf{d}$ and evaluating

$$R(\mathbf{x}) = \frac{I^2(\mathbf{x})}{I(0)} \cos^m \varphi(\mathbf{x}) \left(\frac{z(\mathbf{x}) - z(\mathbf{x} - \Delta\mathbf{d})}{z(\mathbf{x}) + z(\mathbf{x} - \Delta\mathbf{d})} \right)^2 \tag{10}$$

with $I(\mathbf{x})$ the intensity of the sound beam and $\varphi(\mathbf{x})$ the incidence angle at position $\mathbf{x}$. The distance between scan line points is indicated by $\Delta\mathbf{d}$. The exponent m models the heterogeneity of the interface. The reflection coefficient, see Equation (6), is then

$$\rho(\mathbf{x}) = \left(\frac{z(\mathbf{x}) - z(\mathbf{x} - \Delta\mathbf{d})}{z(\mathbf{x}) + z(\mathbf{x} - \Delta\mathbf{d})} \right)^2. \tag{11}$$

The incidence angle, which is the angle between the US beam and the normal of the surface, is calculated with the scalar product

$$\cos \varphi(\mathbf{x}) = \left| \mathbf{d}. \frac{\nabla z(\mathbf{x})}{|\nabla z(\mathbf{x})|} \right| \tag{12}$$

where ∇ is the spatial derivative operator. The intensity is calculated recursively starting from the initial intensity of a sound beam $I(0)$ by

$$I(\mathbf{x}) = I(\mathbf{x} - \Delta\mathbf{d}) \cdot \rho(\mathbf{x}). \tag{13}$$

Finally, a log-compression is applied to the images, so that the reflectivity of the US images $r(\mathbf{x})$ is

$$r(\mathbf{x}) = \frac{\log(1 + a \cdot R(\mathbf{x}))}{\log(1 + a)} \tag{14}$$

with a parameterizing the log-compression. We will use these equations that describe the simulation of the reflectivity part of ultrasound images to reconstruct the impedance in Section 2.3.3.

2.3. Acoustic Impedance Estimation

In this section, we are going to describe the steps for acoustic impedance estimation. First, the images are filtered to reduce speckle. Second, we extract the phase information from the images to identify regions of high reflectivity. Third, we use these regions to reconstruct the impedance for each image, and finally we find the global impedance estimation by averaging acoustic images obtained from each ultrasound image.

2.3.1 Filtering

Dealing with speckle in US images depends on the application. In the majority of cases, speckle is treated as noise, which has to be removed before further processing the images. In a recent work, however, Housden *et al*. [11] use speckle for the registration of consecutive slices in freehand ultrasound. In compounding, where we want to average image information from different viewing angles, speckle patterns are mostly uncorrelated [6]. Also for acoustic impedance estimation, we focus on the regions with high reflectivity and want to ignore speckle from homogeneous parts in between. A multitude of approaches for speckle reduction can be found in the literature such as Gaussian filtering, coherence-enhancing diffusion filtering, and despeckling filters based on the envelope of the US image [6]. We achieved good results with a median filter, which has superior speckle reduction properties compared to Gaussian smoothing [23].

(a) Original US image (b) Phase image (c) Threshold of phase image (d) Impedance estimation (e) Smooth imp. estimation

Figure 4. Processing steps for acoustic impedance estimation of the first forearm image.

(a) Original US image (b) Phase image (c) Threshold of phase image (d) Impedance estimation (e) Smooth imp. estimation

Figure 5. Processing steps for acoustic impedance estimation of the second forearm image.

2.3.2 Phase Calculation

Core to the acoustic impedance estimation is the identification of regions with high reflectivity, indicating a change in acoustic impedance. We use phase information for this purpose because it provides us with structural information independent of the brightness and contrast [8]. For 1-D signals the phase is constructed from the original signal and its Hilbert transform. There are different approaches to extend this concept to N-D. Here we will use the recently introduced *monogenic signal* approach [5]. It uses a generalization of the Hilbert transform, the Riesz transform, to calculate phase information in N-D. The image is filtered by N filters, which are given in the Fourier domain by

$$R_i(f_1, \ldots, f_N) = \frac{f_i}{\sqrt{\sum_{j=1}^{N} f_j^2}} \tag{15}$$

with $f_1, \ldots, f_N$ the Fourier domain coordinates. We follow [7] in applying log-Gabor filters prior to the calculation of the monogenic signal of the image to extract frequency and spatial localization. The monogenic signal provides us with information about the phase and orientation of each pixel, see Figure 2(b) for an example. We threshold the phase image, to get a mask, see Figure 2(c), to extract the reflectivity part from the ultrasound image.

2.3.3 Acoustic Impedance Calculation

Coming back to the ML formulation of our estimation in Equation (5), we see that the reflectivity term in Equation (14) exactly performs the wanted simulation when focusing on the reflection. We will split up the direct estimation of the global impedance z in Equation (5) and, instead, estimate for each US image u_i an acoustic impedance z_i

$$\arg\min_{z_i} \left(u_i(\mathbf{x}) - \frac{\log\left(1 + a \cdot (\cos\varphi(\mathbf{x}))^m \cdot \rho_{z_i}(\mathbf{x})\right)}{\log(1+a)} \right)^2 . \tag{16}$$

In order to perform the optimization, we make the assumption that the incidence angle for the impedance and ultrasound image are roughly the same

$$\cos\varphi(x) = \left| \mathbf{d}. \frac{\nabla z(\mathbf{x})}{|\nabla z(\mathbf{x})|} \right| \approx \left| \mathbf{d}. \frac{\nabla u(\mathbf{x})}{|\nabla u(\mathbf{x})|} \right| . \tag{17}$$

Since the orientation of the interfaces in impedance and ultrasound image should be the same, this approximation is reasonable. Considering, however, that US images are very noisy, this can lead to problems. In our estimation framework, we directly access the orientation information delivered by the phase calculation, which is very robust and accurate, so that the approximation makes sense.

As shown in Equations (8) and (13), the intensity decreases as the ultrasound beam penetrates the tissue farther. However, before the ultrasound images are output, a time-gain compensation (TGC) is applied. The TGC compensates for attenuation of the ultrasound signal received from the tissue interfaces that are farther away from the ultrasound transmitter; simulating that everywhere in the image the same incident intensity is present. Consequently, we ignored the intensity term for the estimation in Equation (16).

The only term in Equation (16) that is still dependent on the acoustic impedance is the reflection coefficient $\rho_{z_i}(\mathbf{x})$.

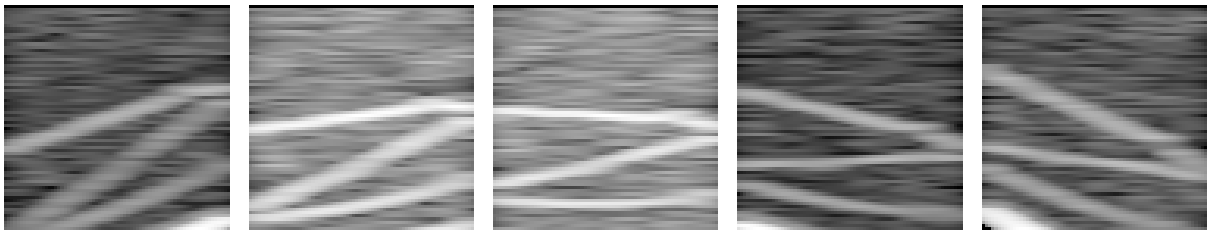

(a) US $-20°$ (b) US $-10°$ (c) US $0°$ (d) US $10°$ (e) US $20°$

Figure 6. Five ultrasound images simulated from CT from $-20°$ to $20°$.

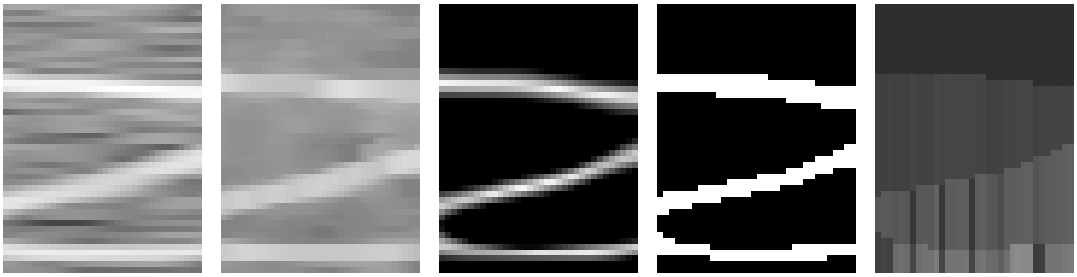

(a) Original US image (b) Filtered image (c) Phase image (d) Thres. of phase img. (e) Imp. estimation

Figure 7. Processing steps for acoustic impedance estimation of simulated ultrasound at $0°$.

Since this term is recursively defined, depending on the previous estimation $z(\mathbf{x} - \Delta\mathbf{d})$, we need an initial value to make the calculation along the scanline. When taking *e.g.* acquisitions in a water bath, we can directly use the acoustic impedance of water. But it is not always possible to acquire a proper initialization and as such, in general, a reconstruction up to a scale is possible. This is sufficient for visualization and US simulation. In the future, further information from the US image such as tissue estimation from RF data [16] or speckle [1] could be integrated to make the estimation more precise.

Since we estimate the acoustic impedance per scanline, an averaging with neighboring scanlines while propagating the values between the interfaces leads to smoother estimations, see Figure 2(e).

2.3.4 Compounding Acoustic Impedance Images

In section 1.2, we argued that compounding of ultrasound images is not a trivial task. In contrast, compounding of estimated acoustic impedance images is straightforward because these images hold a correspondence between intensity value and tissue type. The global acoustic impedance image z is consequently the mean of the estimates z_i at each pixel position. Problems can still occur when structures with high acoustic impedance such as bones cause occlusion in the underlying region. For the detection of occlusions, the intensity term in Equation (13) can be used, to make a reliable compounding possible.

2.4. Visualization

Once the global acoustic impedance image z is estimated, we have to find ways to visualize it for the physician. One possibility would be to directly present the acoustic impedance image, but this may be of limited clinical value, because physicians are not used to these images and may have problems interpreting them. A better way may be to create artificial ultrasound views. The simulation of US from the acoustic impedance image is feasible because it is the acoustic impedance that determines the structure of the US images. It has the advantage, that US views can be simulated that were initially not recorded, and from positions that are physically not possible, *e.g.* below the skin. We use a recently introduced method by Shams *et al.* in [18], designed for simulating ultrasound images from CT data, to simulate US images from acoustic impedance, see Figure 8(h) for an example.

3. Results

We present results for the acoustic impedance estimation for three data sets. The first one is an image of a clay model, see Figure 2(a), the second one consists of two scans of a human forearm, see Figures 4(a) and 5(a), and the third one consists of five simulated US images from a human abdomen, see Figure 6. The acquisitions for the first and second data sets were done in a water bath, because we wanted to avoid tissue deformation due to probe pressure, so that we could focus on the acoustic impedance estimation. We used a linear array ultrasound transducer for the acquisitions.

The steps for acoustic impedance estimation as described

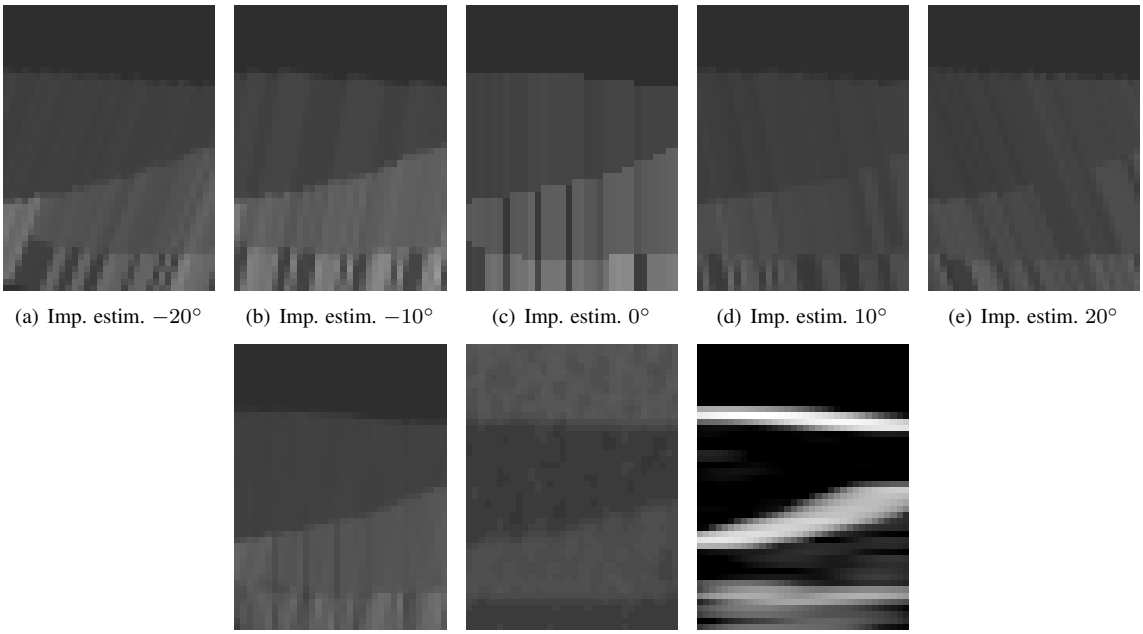

(a) Imp. estim. $-20°$ (b) Imp. estim. $-10°$ (c) Imp. estim. $0°$ (d) Imp. estim. $10°$ (e) Imp. estim. $20°$

(f) Imp. mean (g) CT (h) US from imp. mean

Figure 8. Acoustic impedance estimation in the overlap area from the 5 simulated US images, transformed in reference coordinate system. Mean of estimations, and in comparison the original CT. Simulation of US image from the global acoustic impedance image.

in section 2.3 are shown in Figure 2 for the clay model. The image is filtered with a median filter with a window size 10×10. Then, the phase is calculated on the filtered image, where we use a wavelength of 250mm for the log-Gabor filter, see Figure 2(b). We apply thresholding on the phase image to obtain a mask, showing us the regions with high reflectivity, see Figure 2(c). Determining the threshold is not critical and we performed all our experiments with a value of 0.7. For the calculation of the acoustic impedance, we set log-compression parameter $a = 700$ and the exponent $m = 0.1$. The original and smoothed estimations are shown in Figures 2(d) and 2(e).

In Figures 4 and 5 the estimation steps for both forearm images are shown. We use a wavelength of 180mm for the log-Gabor filter and $a = 1000$ for the log-compression.

For the third data set, we simulate US from a CT image shown in Figure 8(g) using a recently introduced method [18], which produces realistic ultrasound images from CT data. The images are acquired from different viewing angles varying from $-20°$ to $20°$ to create a realistic spatial compounding scenario. We show as an example the processing steps for the estimation of the simulated US images acquired at $0°$ in Figure 7, with a wavelength of 60mm, $a = 83$, and $m = 0.1$. After doing the same with the four remaining images and mapping them back to the reference frame at $0°$, see Figures 8(a) - 8(e), we can calculate the global acoustic impedance image, see Figure 8(f). It is the average of the separate estimations and one clearly sees the improved quality. When comparing it to the original CT image, which can to some respect be seen as ground truth, the good quality of the reconstruction becomes apparent. Finally, we use the global impedance image to simulate an ultrasound image, see Figure 8(h), with the same method we originally used to simulate the US images from CT.

4. Discussion

For the US image of the clay model, we were able to identify the interface and consequently make an estimation of the acoustic impedance. The images of the forearm are pretty noisy, making an exact extraction of the parts with high reflectivity difficult. The extraction of the bone, which is depicted as the half-round structure on the lower left, was correct. In the acoustic impedance estimation of the first forearm we can see that the calculation becomes difficult when structures seem to split, as it is the case on the upper right side of the bone. For the simulated US images the phase extraction worked nicely. Errors in the acoustic impedance estimation of the five images were able to be reduced by averaging them to create a global estimate. When comparing this global estimate to the original CT image, the good quality of the reconstruction becomes apparent. We simulated an ultrasound image from the global estimate at $0°$ rotation, to make it comparable to the original US images, but we could have simulated this from an arbitrary position.

5. Conclusion

We have presented a method to estimate acoustic impedance from multiple ultrasound images. The key to the acoustic impedance calculation is to have a model from the physical imaging process to be able to analyze US images. We have presented such a model and adapted it to the specific needs of acoustic impedance estimation, where we focused on modeling reflections. This allows us to estimate the impedance values at tissue interfaces. We proposed a phase-based image analysis to extract regions of high reflection from the image. Similar to spatial compounding, we average several images to get a robust estimation of the global acoustic impedance. Based on this estimation, we are able to simulate US images from arbitrary positions. Our results show that acoustic impedance estimation is feasible. It would, however, be helpful to integrate further data in the estimation process coming from RF, elastography, and speckle analysis, to make it more reliable. The acoustic impedance image would play a central role for combining these different data sources.

References

[1] S. Aja-Fernandez, M. Martin-Fernandez, and C. Alberola-Lopez. Tissue identification in ultrasound images using rayleigh local parameter estimation. *Bioinformatics and Bioengineering, 2007. BIBE 2007. Proceedings of the 7th IEEE International Conference on*, pages 1129–1133, 14-17 Oct. 2007.

[2] M. Anderson, M. Soo, R. Bentley, and G. Trahey. The detection of breast microcalcifications with medical ultrasound. *The Journal of the Acoustical Society of America*, 101:29, 1997.

[3] V. Behar, D. Adam, and Z. Friedman. A new method of spatial compounding imaging. *Ultrasonics*, 41:377–384, 2003.

[4] C. Dietrich, A. Ignee, M. Gebel, B. Braden, and G. Schuessler. Imaging of the abdomen. *Z Gastroenterol*, 40:965–970, 2002.

[5] M. Felsberg and G. Sommer. The monogenic signal. *IEEE Transactions on Signal Processing*, 49(12):3136–3144, December 2001.

[6] V. Grau, H. Becher, and J. Noble. Registration of multiview real-time 3-d echocardiographic sequences. *Medical Imaging, IEEE Transactions on*, 26(9):1154–1165, Sept. 2007.

[7] V. Grau, H. Becher, and J. A. Noble. Phase-based registration of multi-view real-time three-dimensional echocardiographic sequences. In *International Conference on Medical Image Computing and Computer-Assisted Intervention (MICCAI)*, pages 612–619, 2006.

[8] V. Grau and J. A. Noble. Adaptive multiscale ultrasound compounding using phase information. In *International Conference on Medical Image Computing and Computer-Assisted Intervention (MICCAI)*, pages 589–596, 2005.

[9] W. R. Hedrick, D. L. Hykes, and D. E. Starchman. *Ultrasound Physics and Instrumentation*. Mosby, 4 edition, 2004.

[10] W. Henrich, A. Schmider, S. Kjos, B. Tutschek, and J. W. Dudenhausen. Advantages of and applications for extended field-of-view ultrasound in obstetrics. *Archives of Gynecology and Obstetrics*, V268:121–127, Jun 2003.

[11] R. J. Housden, A. H. Gee, G. M. Treece, and R. W. Prager. Subsample interpolation strategies for sensorless freehand 3d ultrasound. *Ultrasound Med Biol*, 32:1897–904, 2006.

[12] S. Huber, M. Wagner, M. Medl, and H. Czembirek. Real-time spatial compound imaging in breast ultrasound. *Ultrasound Med Biol*, 28(2):155–63, 2002.

[13] S. Jespersen, J. Wilhjelm, and H. Sillesen. In vitro Spatial Compound Scanning for Improved Visualization of Atherosclerosis. *Ultrasound in Medicin and Biology*, 26(8):1357–1362, 2000.

[14] S. H. Kim, B. I. Choi, K. W. Kim, K. H. Lee, and J. K. Han. Extended Field-of-View Sonography: Advantages in Abdominal Applications. *Journal of Ultrasound in Medicine*, 22(4):385–394, 2003.

[15] D. Leotta and R. Martin. Three-dimensional spatial compounding of ultrasound scans with incidence angle weighting. *Ultrasonics Symposium*, 2:1605–1608, 1999.

[16] M. Moradi, P. Mousavi, and P. Abolmaesumi. Tissue characterization using fractal dimension of high frequency ultrasound rf time series. In *International Conference on Medical Image Computing and Computer-Assisted Intervention (MICCAI)*, volume 10, pages 900–908, 2007.

[17] P. Peetrons. Ultrasound of muscles. *European Radiology*, 12(1):35–43, 2002.

[18] R. Shams, R. Hartley, and N. Navab. Real-time simulation of medical ultrasound from CT images. In *International Conference on Medical Image Computing and Computer-Assisted Intervention (MICCAI) (Submitted)*, 2008.

[19] D. Tran, A. Kamani, V. Lessoway, and R. N. Rohling. Adaptive spatial compounding for improving ultrasound images of the epidural space. In S. Y. Emelianov and S. A. McAleavey, editors, *Medical Imaging 2008: Ultrasonic Imaging and Signal Processing*, volume 6513. SPIE, 2008.

[20] C. Wachinger, W. Wein, and N. Navab. Three-dimensional ultrasound mosaicing. In *International Conference on Medical Image Computing and Computer-Assisted Intervention (MICCAI)*, Brisbane, Australia, October 2007.

[21] W. Wein, A. Khamene, D. Clevert, O. Kutter, and N. Navab. Simulation and fully automatic multimodal registration of medical ultrasound. In *International Conference on Medical Image Computing and Computer-Assisted Intervention (MICCAI)*. Springer, Oct. 2007.

[22] J. Wilhjelm, M. Jensen, S. Jespersen, B. Sahl, and E. Falk. Visual and quantitative evaluation of selected image combination schemes in ultrasound spatial compound scanning. *Medical Imaging, IEEE Transactions on*, 23(2):181–190, Feb. 2004.

[23] Z. Yang and M. D. Fox. Speckle reduction and structure enhancement by multichannel median boosted anisotropic diffusion. *EURASIP Journal on Applied Signal Processing*, 2004(1):2492–2502, 2004.